1 **Complex hygroscopic behaviour of ambient aerosol particles revealed by a piezoelectric**
2 **technique**

3 Christi Jose[1,2], Aishwarya Singh[1,2], Kavyashree N. Kalkura[1,2], George V. Jose[3], Shailina Srivastava[1,2],

4 Rameshchand K. A.[4], Shweta Yadav[5], R. Ravikrishna[2,6], M. O. Andreae[7,8,9], Scot T. Martin[10,11],

5 Pengfei Liu[12,*], and Sachin S. Gunthe[1,2,*]

6 [1]Environemntal Engineering Division, Dept of Civil Engineering, Indian Institute of Technology
7 Madras, Chennai 600036, India

8 [2]Centre for Atmospheric and Climate Sciences, Indian Institute of Technology Madras,
9 Chennai 600036, India

10 [3]Dept of Civil Engineering, Indian Institute of Technology Bombay, Mumbai 400076, India

11 [4]Dept of Mechanical Engineering, College of Engineering Munnar, Munnar 685612, India

12 [5]Dept of Environmental Sciences, Central University of Jammu, Samba, Jammu and Kashmir 181143,
13 India

14 [6]Dept of Chemical Engineering, Indian Institute of Technology Madras, Chennai 600036, India

15 [7]Multiphase Chemistry Department, Max Planck Institute for Chemistry, 55128 Mainz, Germany

16 [8]Scripps Institution of Oceanography, University of California San Diego, La Jolla, CA 92093, USA

17 [9]Department of Geology and Geophysics, King Saud University, Riyadh 11451, Saudi Arabia

18 [10]Department of Earth and Planetary Sciences, Harvard University, Cambridge, MA 02138, USA

19 [11]John A. Paulson School of Engineering & Applied Sciences, Harvard University, Cambridge, MA
20 02138, USA

21 [12]School of Earth and Atmospheric Sciences, Georgia Institute of Technology, Atlanta, GA 30332,
22 USA

23 *Correspondence to: Sachin S. Gunthe (s.gunthe@iitm.ac.in) and Pengfei Liu
24 (pengfei.liu@eas.gatech.edu)

25

26 **KEYPOINTS**

27 • QCM technique revealed aerosol properties at low RH values offering insights that
28 may not be captured by traditional size-based measurements

29 • The size-dependent variations in aerosol properties below DRH emphasize the need to
30 understand how aerosol properties change with RH history

31 • Organic in aerosols complicate its cloud forming ability, necessitating additional
32 studies in diverse environments to improve climate models

33 **ABSTRACT**

34 Comprehending the intricate interplay between atmospheric aerosols and water vapour in

35 subsaturated regions is vital for accurate modelling of aerosol–cloud–radiation–climate

36 dynamics. But the microphysical mechanisms governing these interactions with ambient

37 aerosols remain inadequately understood. Here we report results from high-altitude, relatively

38 pristine site in Western-Ghats of India during monsoon, serving as a baseline for climate

39 processes in one of the world's most polluted regions. Utilizing a novel quartz crystal

40 microbalance (QCM) approach, we conducted size-resolved sampling to analyse humidity-

41 dependent growth factors, hygroscopicity, deliquescence behaviour, and aerosol liquid water

42 content (ALWC). Fine-mode aerosols (≤ 2.5 μm) exhibited size-dependent interactions with

43 water vapour, contributing significantly to ALWC. Deliquescence was observed in larger

44 aerosols (>180 nm), influenced by organic species, with deliquescence relative humidity

45 (DRH) lower than that of pure inorganic salts. This research highlights the significance of

46 understanding ambient aerosol-water interactions and hygroscopicity for refining climate

47 models in subsaturated conditions.

48 **PLAIN LANGUAGE SUMMARY**

49 Aerosol particles interact with water vapour in the atmosphere. Understanding these

50 interactions in sub – and super-saturated regions is crucial because they affect processes such

51 as cloud formation, radiation, and climate. We collected ambient aerosol samples from

52 Western Ghats in India to understand natural processes that happen without significant

53 human interventions. Using a special technique involving a quartz crystal sensor, we

54 measured different aspects, such as how aerosols grow with humidity, their ability to uptake

55 the water molecules, and when they transition from solid to liquid (deliquescence).

56 Interestingly, fine particles, especially those smaller than 2.5 μm, exhibited unique

57 behaviours. While larger particles underwent a transition from solid to liquid under certain

58 conditions, this didn't happen for the smaller particles. These findings highlight the

59 importance of understanding these interactions for more accurate climate predictions.

1. INTRODUCTION

Understanding the hygroscopicity of atmospheric aerosols is crucial for assessing cloud formation and their climate and air pollution impact (Cheung et al., 2015). Investigation of the hygroscopicity of ambient aerosols poses significant challenges due to their chemical complexity, particle size variation, phase state, and viscosity. Techniques like Fourier transform infrared spectroscopy (FTIR) (Y. Liu et al., 2008; Y. Liu & Laskin, 2009), quartz crystal microbalance (QCM) (Chao et al., 2020; Demou et al., 2003; P. Liu et al., 2016a; P. Liu, Song, et al., 2018a), Raman spectroscopy (Ling & Chan, 2008; Y. J. Liu et al., 2008), electrodynamic balance (EDB) (Choi & Chan, 2002; Peng & Chan, 2001; Pope et al., 2010), optical microscopy (OM) (Ahn et al., 2010; Eom et al., 2014; Gupta et al., 2015), hygroscopicity tandem differential mobility analysis (HTDMA) (Cheung et al., 2015; Prenni et al., 2007; Zieger et al., 2017a) and size-selected cloud condensation nuclei (CCN) spectrometry (Petters et al., 2007; Pöhlker et al., 2016; Rose et al., 2008) have been employed to study the hygroscopicity of laboratory – generated and ambient aerosols (Tang et al., 2019). However, a consensus on the most effective method is lacking, leading to inconsistent and incomparable results. Hygroscopicity measurements primarily focus on accumulation mode particles, limiting data on nucleation and coarse mode particles with complex behaviours. Discrepancies in hygroscopic properties and organic and inorganic species composition in atmospheric aerosols result in diverse growth factors and phase transitions, crucial for accurate climate modelling (Li et al., 2021).

The QCM is effective in determining mass–based hygroscopicity and physical property variations of atmospherically–relevant aerosols (Demou et al., 2003; P. Liu et al., 2016b; P. Liu, Song, et al., 2018b). It overcomes the limitations of traditional methods like HTDMA, which has a narrow particle size range with limited relative humidity (RH) resolution (Zhao et al., 2022). Conventional HTDMA methods inadequately reveal hygroscopicity heterogeneity and phase transitions in wider aerosol size range, impacting processes like CCN activation and aerosol liquid water (Li et al., 2021). QCM's mass-based measurements accurately quantify aerosol hygroscopicity behaviour across a wide RH range in the atmosphere, detailing physical property variations during phase transitions and help to delineate water uptake mechanisms, including solubility and water diffusion limitations (P. Liu, Li, et al., 2018; P. Liu, Song, et al., 2018b).
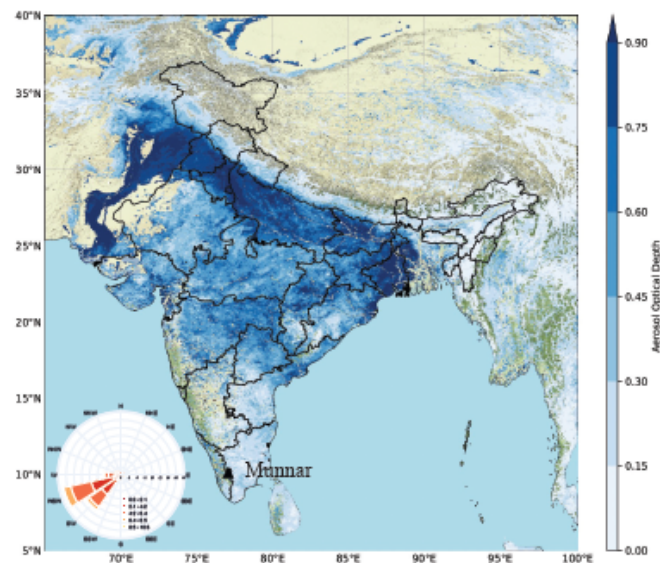
93   India's climate is distinct and intricate, and as per the 2020 climate change assessment report,

94   India has faced challenges like temperature rise and extreme weather events since the mid-

95   20th century. A key hurdle in addressing these issues is the absence of systematic aerosol

96   characteristic measurements, particularly in aerosol-water vapor interactions in the

97   subsaturated regime (Cheung et al., 2015). Aerosol particles from a forest-surrounded by

98   pristine area are anticipated to contain substantial biogenic organic aerosols. The dynamic

99   chemical transformation of secondary organic aerosols (SOA) in the atmosphere leads to

100   intricate compositions. Atmospheric processing further complicates the understanding of

101   phase state and properties of atmospheric aerosols (Rastak et al., 2017). In this study, QCM

102   measurements are utilized to explore aerosol hygroscopicity dependence on RH, chemical

103   composition, and size across a broad range of ambient aerosols in India's relatively pristine

104   setting.

105   **2. MATERIALS AND METHODS**

106   Size-resolved ambient aerosols were sampled at the Natural Aerosol and Bioaerosol High

107   Altitude (NABHA) Laboratory at the College of Engineering, Munnar (10.0930° N, 77.0682°

108   E; 1600 m above mean sea level), a high-altitude and typically clean site situated in the

109   Western Ghats of India, using a 10-stage micro-orifice uniform deposit impactor (MOUDI-II

110   120-R, TSI) (V. Marple et al., 2014; V. A. Marple et al., 1991) during the monsoon season

111   (August-September) of 2021. Ambient particles collected on PTFE (Polytetrafluoroethylene)

112   filters were transferred to a hydrophobic SiO_2-coated quartz sensor by gently pressing the

113   filter paper onto the sensor. The hygroscopic growth factor, hygroscopicity parameter and

114   deliquescence relative humidity (DRH) were estimated using a highly sensitive mass balance

115   instrument, QCM (QSense Analyzer, Biolin Scientific) (P. Liu, Song, et al., 2018a; Reviakine

116   et al., 2011). The accuracy and robustness of the method were demonstrated by performing

117   measurements of the hygroscopic growth factor and DRH for sucrose and $(NH_4)_2SO_4$

118   particles, respectively, which were compared with previously reported results (Arenas et al.,

119   2012a; Chao et al., 2020; Martin, 2000; Norrish, 1966; Peng et al., 2022; Starzak & Peacock,

120   1997; Zobrist et al., 2011) (Fig. S3 and S4). The hygroscopic growth factor and the

121   corresponding hygroscopicity parameter, κ, were determined over a wide range of RH

122   conditions using κ-Köhler theory (Petters & Kreidenweis, 2007), where κ represents a

123   quantitative measure of aerosol water uptake characteristics and CCN activity (Zhao et al.,

124   2022). The water uptake characteristics and the phase transition behaviours of the ambient

125   samples were investigated and compared between different size ranges of particles below 10

126   µm collected using the MOUDI sampler. The Aerosol Liquid Water Content (ALWC) (Bian

127   et al., 2014) at different RH conditions was also estimated from corresponding hygroscopicity

128   parameters for each size range of particles (Fig. S5). The number size distributions of the

129   ambient aerosol particles of size 10 to 420 nm [measured in parallel using a scanning

130   mobility particle sizer – SMPS, comprised of an electrostatic classifier (EC, TSI Model 3082)

131   equipped with a differential mobility analyser (DMA, TSI Model 3081) and a condensation

132   particle counter (CPC, TSI Model 3750)], were then converted to mass size distributions

133   assuming a particle density of 1.2 g cm^{-3} (DeCarlo et al., 2004). The supermicron particle

134   mass size distribution for the same season, but a different year, was used in this study, which

135   had been obtained using an Ultraviolet Aerodynamic Particle Sizer (UV-APS, TSI Inc.,

136   model 3314) (Valsan et al., 2016).

137

138   Meteorological parameters were recorded using an automatic weather station (AWS, Clima

139   Sensor US) during the sampling period. Figure 1 shows the sampling site – Munnar, along

140   with aerosol optical depth (AOD) over India during the monsoon season, indicating the

141   relatively pristine nature of the sampling site. During the measurement, airmasses

142   predominantly arrived from the southwest direction, bringing clean marine influx to the

143   observational site and resulting in a low influence of anthropogenic emissions (Fig. 1).

144   A more detailed description of the instruments, experimental techniques, and estimation of

145   various parameters is provided in the Supporting Information (SI).

146

147
148
149
150
151
152
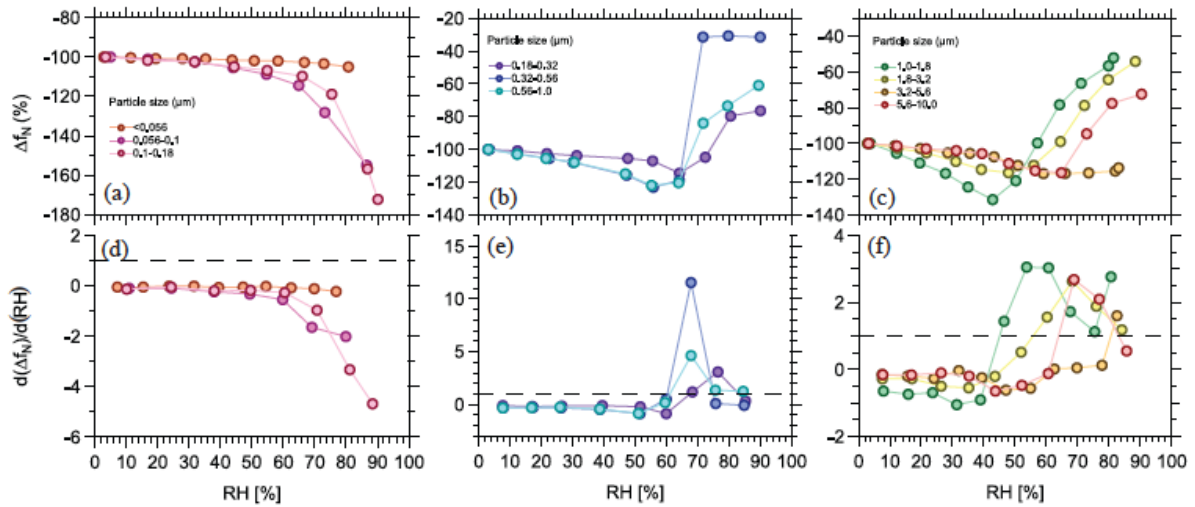153
154
155
156
157
158
159
160
161
162
163
164
165

Figure 1. Spatial distribution of average Aerosol Optical Depth (AOD) derived from MODIS (Moderate Resolution Imaging Spectroradiometer) Level 2 data over the Indian continental region during the monsoon season of 2021 (June - September). The AOD distribution clearly indicates a relatively low aerosol loading over the observational site of Munnar (marked as a black triangle) compared with the other parts of India. The wind rose diagram shown in the inset shows the average wind speed and wind direction arriving at the sampling site during the ambient aerosol sampling period (August – September 2021). The prevailing air masses mostly originated over the Indian Ocean and arrived from southwest direction, bringing clean marine influx to the observational site, confirming the relatively low influence of anthropogenic activities.

3. RESULTS AND DISCUSSION

The QCM sensor's oscillation frequency variation (Δf) signifies water uptake and release, providing insights into adsorption, desorption, and physical states of particles during solid-to-aqueous phase transition (Arenas et al., 2012b). Normalizing the frequency shift at higher RH to that of deposited dry sample (RH <5%) yields the percentage value, Δf_N (Chao et al., 2020). Figure 2 shows Δf_N for the ambient aerosol particles across various RH levels and sampled size ranges. A negative sign in Δf_N indicates frequency reduction with increasing RH due to water uptake. Further details of Δf_N and its derivative, $d(\Delta f_N)/(RH)$, are available in SI.

For the particle size <180 nm (Fig. 2a), Δf_N decreased, implying water uptake, with <56 nm particles exhibiting the lowest value. In Figure 2b and 2c, particles showed increased water uptake at lower RH, evidenced by Δf_N decrease. However, Δf_N suddenly increased at specific RH, indicating a drastic water uptake leading to deliquescence-induced phase transition. Figures 2a-c revealed deliquescence in particles >180 nm at different RH (known as DRH), absent in those <180 nm. Past studies reported no deliquescence for ambient and laboratory-generated atmospherically relevant particles even at high RH, attributing them to organic nature (Arenas et al., 2012a; Brooks et al., 2002; Chao et al., 2020; Peng et al., 2022). We hypothesize that particles <180 nm were likely dominated by freshly formed secondary organic aerosols (SOA) from biogenic volatile organic compound (VOC) oxidation, supported by the densely vegetated/forest region and season. Concurrent quasi-continuous measurements during the same campaign indicated upto ~90% organic fraction in NR-PM$_1$ (non-refractory particulate matter with an aerodynamic diameter ≤1 μm; Tab. S2) with details discussed in subsequent studies.

198

199 **Figure 2.** Deliquescence phase transition behaviour of size-resolved ambient aerosol particles from Munnar. For
200 panels a, b, and c, Δf_N represents the change in the oscillation frequency of the quartz crystal microbalance
201 (QCM) sensor resulting due to water uptake by the ambient aerosol particles at different relative humidity (RH)
202 conditions normalized to that of the dry aerosol particles at RH <5%, expressed as percentage. The decrease in
203 the value of Δf_N for each size range for the sampled ambient aerosol particles indicates the water uptake at
204 different RH conditions in the subsaturated regime. The solid markers and lines identify different particle size
205 ranges. In panels d, e, and f, the derivative of Δf_N with respect to RH (d(Δf_N)/d(RH)) is plotted against RH to
206 determine the deliquescence relative humidity (DRH) value corresponding to the respective aerosol size ranges.
207 The RH values at which d(Δf_N)/d(RH) becomes ≥1 (marked by the dotted line) represent the DRH values for the
208 individual aerosol size ranges.

209

210 Following Chao et al. (2020), DRH, indicated by d(Δf_N)/(RH) ≥1 ranged from ~60 – 68% for

211 three size ranges (180 nm – 320 nm; 320 nm – 560 nm; 560 nm – 1 μm) in this study (Fig.

212 2e). Above 180 nm, inorganic salts, like $(NH_4)_2SO_4$, may contribute to DRH appearance (Hu

213 et al., 2010) (Fig. 2b,e). These DRH values, smaller than pure $(NH_4)_2SO_4$ (DRH=80%),

214 suggest mixed salts and/or organic compounds in the sampled aerosol particles. The

215 deliquescence behaviour of organic-inorganic mixtures introduces complexity due to

216 solubility limitations, influenced by the organic species in the aerosol particles. Previous

217 studies noted reduced DRH of inorganic species and sometimes, unaffected by organics

218 (Smith et al., 2011, 2012, 2013). Thus, we hypothesize 180 nm to 1 μm particles at this site

219 reflect a complex mixture of inorganic salts like $(NH_4)_2SO_4$ and water-soluble organic

220 compounds. Supermicron particles (>1 μm), except 1 – 1.8 μm, showed <17% Δf_N, indicating

221 lower water uptake (Fig. 2c). Beyond maximum water uptake, the three size ranges exhibited

222 different DRH values. 1.8 – 3.2 μm and 5.6 – 10 μm exhibited DRH between 56 – 68%,

223 suggesting a mixture of water-soluble organic compounds and inorganic salts. However, 3.2

224 – 5.6 μm showed a very high DRH (>81%) with the organic fraction minimally affecting

225 DRH due to solubility limitations. For 1.8 – 3.2 μm and 5.6 – 10 μm, reduced DRH
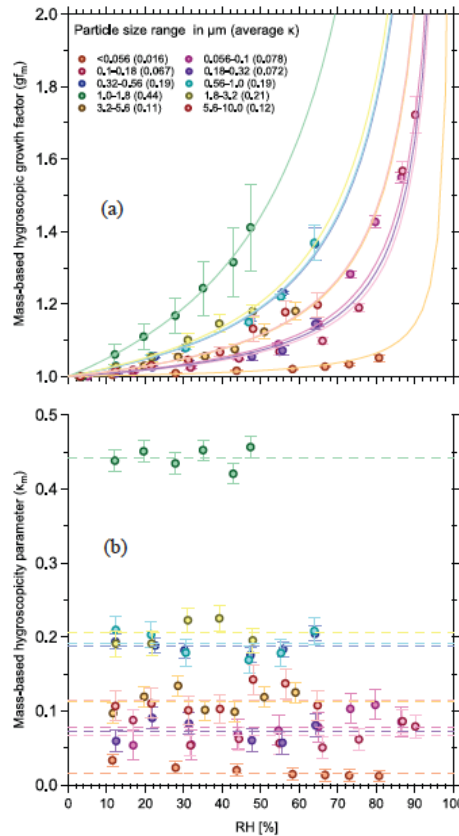
226   compared to pure inorganic salts suggests a mix of water-soluble organic and inorganic

227   compounds (Smith et al., 2011, 2012, 2013). The $1.0 - 1.8$ μm range exhibited a $>30\%$ Δf_N

228   reduction at ~42% RH, indicating a higher water uptake and the observed DRH appeared to

229   be ~45 – 53%, consistent with the highest κ_m (~0.44, see discussion below) among all

230   measured size ranges (Chao et al., 2020). The low DRH at this site suggests presence of

231   highly water-soluble organic material within the organic-inorganic (sea salt) mixture in this

232   size range.

233

234   Figure 3 shows the size-resolved mass-based hygroscopic growth factors (gf_m) and the

235   corresponding mass-based hygroscopicity parameters (κ_m) of ambient aerosol particles

236   calculated from QCM measurements (Text S4 and S5) over a wide RH range (2 – 90%). In

237   Figure 3a, the growth factor increases with water uptake in humid air, showing size-

238   dependent variations across different RH levels (indicated by markers). Each size range had a

239   maximum RH limit beyond which gf_m estimation was impossible due to deliquescence, as

240   observed in previous studies (Chao et al., 2020). Accordingly, the highest $gf_m=1.72$ was

241   recorded at RH=90% for the $100 - 180$ nm particles. The pronounced variations in gf_m

242   between different-sized particles at a given RH indicate varying chemical composition and

243   hygroscopicity across the sampled sizes.

244

245   Figure 3b shows the size-dependent average κ_m values, calculated from the gf_m values in

246   Figure 3a. Each particle size range exhibited minimal κ_m variation (average $\kappa_m \pm 0.007$),

247   suggesting ideal solution behaviour across the wide RH range (Z. Wang et al., 2017). The

248   average κ_m values (indicated by dashed lines in Figure 3b) of the size-resolved ambient

249   particles varied significantly between 0.016 (<0.056 nm) and 0.44 ($1.0 - 1.8$ μm) over the

250   investigated RH range. This implies κ_m as a function of size, and indicates distinct chemical

251   compositions for each size fraction. For example, the small increase in κ_m from 0.016 to

252   0.078 for particles <56 nm to 56-100 nm, respectively, is potentially owing to aging

253   processes (Zhang et al., 2023). Aerosol particles <320 nm exhibited very low average κ_m

254   (0.06), which may be primarily due to the strong dominance of organic compounds in these

255   size ranges (Demou et al., 2003; Li et al., 2021; Shi et al., 2022). The particles in the size

256   range of 320 nm – 1 μm were moderately hygroscopic (average $\kappa_m=0.19$) indicating the

257   influence of inorganic salts (Wu et al., 2016). The particles between $1.0 - 1.8$ μm exhibited

258   highest κ_m (0.44), which implies the presence of highly hygroscopic material such as sea salt
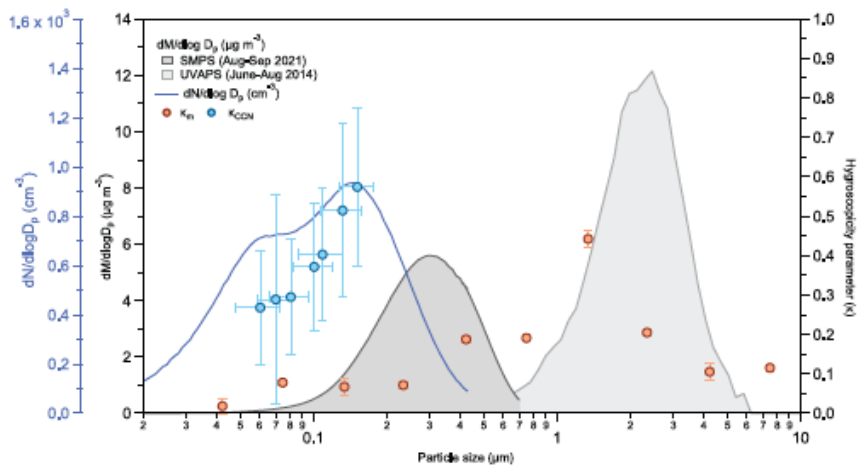
259 (Zieger et al., 2017b) mixed with organic compounds. Even larger particles exhibited reduced

260 κ_m, possibly due to the presence of dust particles (Koehler et al., 2009), transported at this site

261 during monsoon season (Valsan et al., 2016). The κ-Köhler parameterization fit accurately

262 elucidates the gf_m within each size range over a wide range of RH values (Petters &

263 Kreidenweis, 2007).

264

Figure 3. Size-resolved hygroscopicity measurements of ambient aerosol particles at the high-altitude site,
Munnar, during the Monsoon season (August-September 2021). (a) Mass-based hygroscopic growth factor (gf_m)
derived using a quartz crystal microbalance (QCM) for ten different size ranges of ambient aerosol particles at
different relative humidity (RH) conditions in the subsaturated regime (circles). The solid lines represent the
corresponding κ-Köhler growth factor fits obtained using the mean value of mass-based hygroscopicity
parameters, κ_m. The error bars represent the variations in gf_m averaged over the mass change corresponding to
different overtone frequencies of the QCM sensor at respective RH conditions. The values in parentheses are the
mean κ_m values corresponding to the respective size ranges. (b) The data points are the κ_m values calculated
based on the gf_m (as shown in (a)) using the κ-Köhler theory for different RH conditions in the subsaturated
regime. The dotted lines represent the mean κ_m value for each size range of ambient aerosol particles and the
error bars represent one standard deviation.

304 Figure 4 shows the size dependency of κ_m in the subsaturated regime measured by QCM

305 together with κ_{CCN} (Text S2) in the supersaturated regime determined by size-resolved CCN

306 measurements and aerosol size distributions obtained by SMPS and UV-APS. The submicron

307 particles show a bimodal number size distribution with an Aitken mode peak at 63 nm and an

308 accumulation mode at 145 nm, while the mass size distributions peak at 350 nm and 3 µm,

309   respectively. The average κ_{CCN} increased from a value of 0.28 for the Aitken mode particles

310   to 0.47 for the accumulation mode particles. In the submicron region, κ_m exhibited a nominal

311   increase with particle size (Wu et al., 2016). in parallel with the increase in κ_{CCN}, albeit at

312   much lower absolute values. This increase likely reflects the decrease of organic fraction with

313   size in the submicron range, which is supported by the appearance of deliquescence in the

314   size range above 180 nm, indicating the presence of inorganic salts. In the supermicron

315   region (for particles ≥1 µm), κ_m peaked due to the potential presence of NaCl particles in the

316   size range 1.0 – 1.8 µm, and decreased again in the higher size ranges (>1.8 µm) likely

317   because of the presence of dust particles. The average κ_m value (0.18) obtained from QCM

318   measurements across all the sampled size ranges in the subsaturated regime was lower than

319   the average κ_{CCN} (0.39), likely due to the solubility limitation (Dusek et al., 2011; Hersey et

320   al., 2013; Rastak et al., 2017; Riipinen et al., 2015; Wittbom et al., 2018) of organic and

321   inorganic compounds in ambient aerosol particles below the DRH. Most inorganic species

322   are completely dissolved beyond the DRH point in the subsaturated regime, allowing κ_{CCN} to

323   assume complete particle solubility (Pajunoja et al., 2015; Petters & Kreidenweis, 2007).

324

325
326
327
328
329
330
331
332
333
334
335
336
337
338
339

340   **Figure 4.** Aerosol size distributions, hygroscopicity parameters derived from quartz crystal microbalance
341   (QCM) experiments (κ_m), and from size-resolved cloud condensation nuclei (CCN) measurements (κ_{CCN}). The
342   number size distribution obtained using a Scanning Mobility Particle Sizer (SMPS) over the size range of 10 –
343   430 nm (blue curve) was measured during the sampling period and exhibited a bimodal distribution. The mass
344   size distributions (dark grey shaded area) were derived based on the aerosol number size distribution by
345   assuming a density of 1.2 g cm^{-3} for the submicron region. The mass size distribution for the supermicron range
346   (light grey shaded area) was obtained using Ultraviolet Aerodynamic Particle Sizer (UV-APS) measurements
347   during the same season (June-August) but for a different year (2014). The hygroscopicity parameters derived
348   from QCM experiments (κ_m; orange points) and size-resolved CCN measurements (κ_{CCN}; blue points) are shown
349   for the comparison. The error bars for κ_m and κ_{CCN} indicate the measurement uncertainty and variability,
350   respectively.

351

352   Unlike QCM measurements, the hygroscopicity parameters obtained in previous studies

353   using the HTDMA technique (κ_{HTDMA}) are often consistent with κ_{CCN}, as the particle

354   hygroscopicity is determined by particle size increase above DRH point, unaffected by

355   solubility limits (Pajunoja et al., 2015; Y. Wang et al., 2018; Wu et al., 2013). The technical

356   limitations, particularly limited diameter changes corresponding to gf_m values less than 2.0,

357   prevent HTDMA from measuring aerosol hygroscopic properties below the DRH point in the

358   subsaturated regime (Laskina et al., 2015). In contrast, the QCM technique, which is not

359   subject to these limitations, can be used to understand the water uptake characteristics of

360   aerosol particles in the subsaturated regime below DRH and substantially enhance our

361   understanding about solubility limitations of organic and inorganic compounds in the lower

362   RH region. Such an enhancement in the knowledge is crucial for accurately quantifying the

363   radiative forcing effects of ambient aerosol particles in the atmosphere. The strong size

364   dependence of κ_m also indicated varying chemical composition for different size ranges

365   measured in this study.

4. SUMMARY AND ATMOSPHERIC IMPLICATIONS

367   We report the first results based on a high-sensitivity QCM technique to investigate the mass-

368   based growth factor and hygroscopicity parameter of size–resolved ambient aerosols over a

369   wide range of RH from a relatively pristine high–altitude site in India. For the investigated

370   size ranges, the pronounced variations in gf_m below the DRH provided an opportunity to

371   better understand the changes in ambient aerosol properties even at low RH values, which

372   may not be revealed by size-based growth factor measurements (Hu et al., 2010; Laskina et

373   al., 2015). These measurements clearly highlight the important and critical role in knowing

374   the changes in aerosol properties based on their RH history for an improved understanding of

375   water uptake, phase transition, and radiative impact of atmospheric aerosol particles (Zhao et

376   al., 2022). Based on the estimated κ_m values, the ambient aerosol particles exhibited the

377   behaviour of an ideal solution (Pajunoja et al., 2015) and strong size-dependent chemical

378   composition. We further observed a pronounced size dependency of the DRH values

379   potentially resulting from complexities of organic solubility in organic–inorganic mixtures

380   (Li et al., 2021). Such a complexity owing to the presence of various organic species may

381   alter the CCN behaviour of atmospheric aerosol particles due to phase transitions and

382   changes in physical properties. The understanding of CCN activation in the supersaturated

383   regime under the assumption of complete solubility of particles is relatively well established.

384   But the understanding of the thermodynamic properties associated with particle growth in the

385   subsaturated regime still remains a challenge. Our findings emphasize the need for additional

386   experiments on ambient and atmospherically relevant laboratory-generated aerosol particles

387   using high-sensitivity techniques like QCM. We demonstrated the importance of this

388   technique to better understand the rapid changes in aerosol properties resulting from exposure

389   to a wide range of atmospheric RH conditions. The enhancement in our understanding of the

390   complex interplay between water vapour and aerosol particles will help in developing more

391   accurate models to effectively describe the role of aerosols in atmospheric processes to

392   reduce climate uncertainties and assess the impact of air pollution on human and ecosystem

393   health.

ASSOCIATED CONTENT

Author contributions

SSG conceived the idea. SSG and PL conceptualized the study and designed the research. CJ further developed and validated the QCM measurements for the ambient aerosol studies. CJ performed the field measurement campaign to collect the aerosol samples with support from AS, KNK, and RKA. CJ performed all the laboratory experiments using QCM with support from SS. GVJ performed the satellite data analysis to obtain the AOD values. CJ carried out the data analysis obtained from QCM with input from PL and SSG. CJ and AS performed the scientific interpretation of the QCM data under the mentorship of RR, SSG and PL. CJ wrote the first draft of manuscript under the mentorship of SSG with inputs from PL and RR, and further edits from SY. MOA and STM further provided critical and valuable inputs on the manuscript.

Open research

The data used in the manuscript has been deposited in an open research repository as Excel files, accessible at https://doi.org/10.6084/m9.figshare.24512377. MODIS data were sourced from the Level 2 and Atmosphere Archive and Distribution System (LAADS) (https://doi.org/10.5067/MODIS/MYD04_3K.061). Figures were prepared using Igor Pro version 9 (WaveMetrics Inc.), licensed by SSG and accessible at https://www.wavemetrics.com/software/igor-pro-9.

References

433 **References**

434 Ahn, K. H., Kim, S. M., Jung, H. J., Lee, M. J., Eom, H. J., Maskey, S., & Ro, C. U. (2010).
435   Combined use of optical and electron microscopic techniques for the measurement of
436   hygroscopic property, chemical composition, and morphology of individual aerosol particles.
437   *Analytical Chemistry*, *82*(19), 7999–8009. https://doi.org/10.1021/ac101432y

438 Arenas, K. J. L., Schill, S. R., Malla, A., & Hudson, P. K. (2012a). Deliquescence phase transition
439   measurements by quartz crystal microbalance frequency shifts. *Journal of Physical Chemistry A*,
440   *116*(29), 7658–7667. https://doi.org/10.1021/jp3016722

441 Arenas, K. J. L., Schill, S. R., Malla, A., & Hudson, P. K. (2012b). Deliquescence phase transition
442   measurements by quartz crystal microbalance frequency shifts. *Journal of Physical Chemistry A*,
443   *116*(29), 7658–7667. https://doi.org/10.1021/jp3016722

444 Bian, Y. X., Zhao, C. S., Ma, N., Chen, J., & Xu, W. Y. (2014). A study of aerosol liquid water
445   content based on hygroscopicity measurements at high relative humidity in the North China
446   Plain. *Atmospheric Chemistry and Physics*, *14*(12), 6417–6426. https://doi.org/10.5194/acp-14-
447   6417-2014

448 Brooks, S. D., Wise, M. E., Cushing, M., & Tolbert, M. A. (2002). Deliquescence behavior of
449   organic/ammonium sulfate aerosol. *Geophysical Research Letters*, *29*(19).
450   https://doi.org/10.1029/2002GL014733

451 Chao, H. J., Huang, W. C., Chen, C. L., Chou, C. C. K., & Hung, H. M. (2020). Water Adsorption vs
452   Phase Transition of Aerosols Monitored by a Quartz Crystal Microbalance. *ACS Omega*, *5*(49),
453   31858–31866. https://doi.org/10.1021/acsomega.0c04698

454 Cheung, H. H. Y., Yeung, M. C., Li, Y. J., Lee, B. P., & Chan, C. K. (2015). Relative Humidity-
455   Dependent HTDMA Measurements of Ambient Aerosols at the HKUST Supersite in Hong
456   Kong, China. *Aerosol Science and Technology*, *49*(8), 643–654.
457   https://doi.org/10.1080/02786826.2015.1058482

458 Choi, M. Y., & Chan, C. K. (2002). The effects of organic species on the hygroscopic behaviors of
459   inorganic aerosols. *Environmental Science and Technology*, *36*(11), 2422–2428.
460   https://doi.org/10.1021/es0113293

461 DeCarlo, P. F., Slowik, J. G., Worsnop, D. R., Davidovits, P., & Jimenez, J. L. (2004). Particle
462   morphology and density characterization by combined mobility and aerodynamic diameter
463   measurements. Part 1: Theory. *Aerosol Science and Technology*, *38*(12), 1185–1205.
464   https://doi.org/10.1080/027868290903907

465 Demou, E., Visram, H., Donaldson, D. J., & Makar, P. A. (2003). Uptake of water by organic films:
466   The dependence on the film oxidation state. *Atmospheric Environment*, *37*(25), 3529–3537.
467   https://doi.org/10.1016/S1352-2310(03)00430-8

468 Dusek, U., Frank, G. P., Massling, A., Zeromskiene, K., Iinuma, Y., Schmid, O., Helas, G., Hennig,
469   T., Wiedensohler, A., & Andreae, M. O. (2011). Water uptake by biomass burning aerosol at
470   sub-and supersaturated conditions: Closure studies and implications for the role of organics.
471   *Atmospheric Chemistry and Physics*, *11*(18), 9519–9532. https://doi.org/10.5194/acp-11-9519-
472   2011

473 Eom, H. J., Gupta, D., Li, X., Jung, H. J., Kim, H., & Ro, C. U. (2014). Influence of collecting
474   substrates on the characterization of hygroscopic properties of inorganic aerosol particles.
475   *Analytical Chemistry*, *86*(5), 2648–2656. https://doi.org/10.1021/ac4042075

Gupta, D., Kim, H., Park, G., Li, X., Eom, H. J., & Ro, C. U. (2015). Hygroscopic properties of NaCl and NaNO3 mixture particles as reacted inorganic sea-salt aerosol surrogates. *Atmospheric Chemistry and Physics*, *15*(6), 3379–3393. https://doi.org/10.5194/acp-15-3379-2015

Hersey, S. P., Craven, J. S., Metcalf, A. R., Lin, J., Lathem, T., Suski, K. J., Cahill, J. F., Duong, H. T., Sorooshian, A., Jonsson, H. H., Shiraiwa, M., Zuend, A., Nenes, A., Prather, K. A., Flagan, R. C., & Seinfeld, J. H. (2013). Composition and hygroscopicity of the Los Angeles Aerosol: CalNex. *Journal of Geophysical Research Atmospheres*, *118*(7), 3016–3036. https://doi.org/10.1002/jgrd.50307

Hu, D., Qiao, L., Chen, J., Ye, X., Yang, X., Cheng, T., & Fang, W. (2010). Hygroscopicity of inorganic aerosols: Size and relative humidity effects on the growth factor. *Aerosol and Air Quality Research*, *10*(3), 255–264. https://doi.org/10.4209/aaqr.2009.12.0076

Koehler, K. A., Kreidenweis, S. M., DeMott, P. J., Petters, M. D., Prenni, A. J., & Carrico, C. M. (2009). Hygroscopicity and cloud droplet activation of mineral dust aerosol. *Geophysical Research Letters*, *36*(8), 1–5. https://doi.org/10.1029/2009GL037348

Laskina, O., Morris, H. S., Grandquist, J. R., Qin, Z., Stone, E. A., Tivanski, A. V., & Grassian, V. H. (2015). Size Matters in the water uptake and hygroscopic growth of atmospherically relevant multicomponent aerosol particles. *Journal of Physical Chemistry A*, *119*(19), 4489–4497. https://doi.org/10.1021/jp510268p

Li, W., Teng, X., Chen, X., Liu, L., Xu, L., Zhang, J., Wang, Y., Zhang, Y., & Shi, Z. (2021). Organic Coating Reduces Hygroscopic Growth of Phase-Separated Aerosol Particles. *Environmental Science and Technology*, *55*(24), 16339–16346. https://doi.org/10.1021/acs.est.1c05901

Ling, T. Y., & Chan, C. K. (2008). Partial crystallization and deliquescence of particles containing ammonium sulfate and dicarboxylic acids. *Journal of Geophysical Research Atmospheres*, *113*(14). https://doi.org/10.1029/2008JD009779

Liu, P., Li, Y. J., Wang, Y., Bateman, A. P., Zhang, Y., Gong, Z., Bertram, A. K., & Martin, S. T. (2018). Highly Viscous States Affect the Browning of Atmospheric Organic Particulate Matter. *ACS Central Science*, *4*(2), 207–215. https://doi.org/10.1021/acscentsci.7b00452

Liu, P., Li, Y. J., Wang, Y., Gilles, M. K., Zaveri, R. A., Bertram, A. K., & Martin, S. T. (2016a). Lability of secondary organic particulate matter. *Proceedings of the National Academy of Sciences of the United States of America*, *113*(45), 12643–12648. https://doi.org/10.1073/pnas.1603138113

Liu, P., Li, Y. J., Wang, Y., Gilles, M. K., Zaveri, R. A., Bertram, A. K., & Martin, S. T. (2016b). Lability of secondary organic particulate matter. *Proceedings of the National Academy of Sciences of the United States of America*, *113*(45), 12643–12648. https://doi.org/10.1073/pnas.1603138113

Liu, P., Song, M., Zhao, T., Gunthe, S. S., Ham, S., He, Y., Qin, Y. M., Gong, Z., Amorim, J. C., Bertram, A. K., & Martin, S. T. (2018a). Resolving the mechanisms of hygroscopic growth and cloud condensation nuclei activity for organic particulate matter. *Nature Communications*, *9*(1). https://doi.org/10.1038/s41467-018-06622-2

Liu, P., Song, M., Zhao, T., Gunthe, S. S., Ham, S., He, Y., Qin, Y. M., Gong, Z., Amorim, J. C., Bertram, A. K., & Martin, S. T. (2018b). Resolving the mechanisms of hygroscopic growth and cloud condensation nuclei activity for organic particulate matter. *Nature Communications*, *9*. https://doi.org/10.1038/s41467-018-06622-2

Liu, Y. J., Zhu, T., Zhao, D. F., & Zhang, Z. F. (2008). Investigation of the hygroscopic properties of Ca(NO3) 2 and internally mixed Ca(NO3)2/CaCO 3 particles by micro-Raman spectrometry. *Atmospheric Chemistry and Physics*, 8(23), 7205–7215. https://doi.org/10.5194/acp-8-7205-2008

Liu, Y., & Laskin, A. (2009). *Hygroscopic Properties of CH3SO3Na, CH3SO3NH4, (CH3SO3)2Mg, and (CH3SO3)2Ca Particles Studied by micro-FTIR Spectroscopy*. 1531–1538.

Liu, Y., Yang, Z., Desyaterik, Y., Gassman, P. L., Wang, H., & Laskin, A. (2008). Hygroscopic behavior of substrate-deposited particles studied by micro-FT-IR spectroscopy and complementary methods of particle analysis (Analytical Chemistry (2008) 80, (633-642)). *Analytical Chemistry*, 80(18), 7179. https://doi.org/10.1021/ac801397q

Marple, V. A., Rubow, K. L., & Behm, S. M. (1991). A microorifice uniform deposit impactor (moudi): Description, calibration, and use. *Aerosol Science and Technology*, 14(4), 434–436. https://doi.org/10.1080/02786829108959504

Marple, V., Olson, B., Romay, F., Hudak, G., Geerts, S. M., & Lundgren, D. (2014). Second generation micro-orifice uniform deposit impactor, 120 MOUDI-II: Design, Evaluation, and application to long-term ambient sampling. *Aerosol Science and Technology*, 48(4), 427–433. https://doi.org/10.1080/02786826.2014.884274

Martin, S. T. (2000). Phase transitions of aqueous atmospheric particles. *Chemical Reviews*, 100(9), 3403–3453. https://doi.org/10.1021/cr990034t

Norrish, R. (1966). Equation for the activity coefficients and equilibrium relative humidities. *JInternational Journal of Food Science & Technology*, 1, 25–39.

Pajunoja, A., Lambe, A. T., Hakala, J., Rastak, N., Cummings, M. J., Brogan, J. F., Hao, L., Paramonov, M., Hong, J., Prisle, N. L., Malila, J., Romakkaniemi, S., Lehtinen, K. E. J., Laaksonen, A., Kulmala, M., Massoli, P., Onasch, T. B., Donahue, N. M., Riipinen, I., … Virtanen, A. (2015). Adsorptive uptake of water by semisolid secondary organic aerosols. *Geophysical Research Letters*, 42(8), 3063–3068. https://doi.org/10.1002/2015GL063142

Peng, C., & Chan, C. K. (2001). The water cycles of water-soluble organic salts of atmospheric importance. *Atmospheric Environment*, 35(7), 1183–1192. https://doi.org/10.1016/S1352-2310(00)00426-X

Peng, C., Chen, L., & Tang, M. (2022). A database for deliquescence and efflorescence relative humidities of compounds with atmospheric relevance. *Fundamental Research*, 2(4), 578–587. https://doi.org/10.1016/j.fmre.2021.11.021

Petters, M. D., & Kreidenweis, S. M. (2007). A single parameter representation of hygroscopic growth and cloud condensation nucleus activity. *Atmospheric Chemistry and Physics*, 7(8), 1961–1971. https://doi.org/10.5194/acp-7-1961-2007

Petters, M. D., Prenni, A. J., Kreidenweis, S. M., & DeMott, P. J. (2007). On measuring the critical diameter of cloud condensation nuclei using mobility selected aerosol. *Aerosol Science and Technology*, 41(10), 907–913. https://doi.org/10.1080/02786820701557214

Pöhlker, M. L., Pöhlker, C., Ditas, F., Klimach, T., De Angelis, I. H., Araújo, A., Brito, J., Carbone, S., Cheng, Y., Chi, X., Ditz, R., Gunthe, S. S., Kesselmeier, J., Könemann, T., Lavrič, J. V., Martin, S. T., Mikhailov, E., Moran-Zuloaga, D., Rose, D., … Pöschl, U. (2016). Long-term observations of cloud condensation nuclei in the Amazon rain forest - Part 1: Aerosol size distribution, hygroscopicity, and new model parametrizations for CCN prediction. *Atmospheric Chemistry and Physics*, 16(24), 15709–15740. https://doi.org/10.5194/acp-16-15709-2016
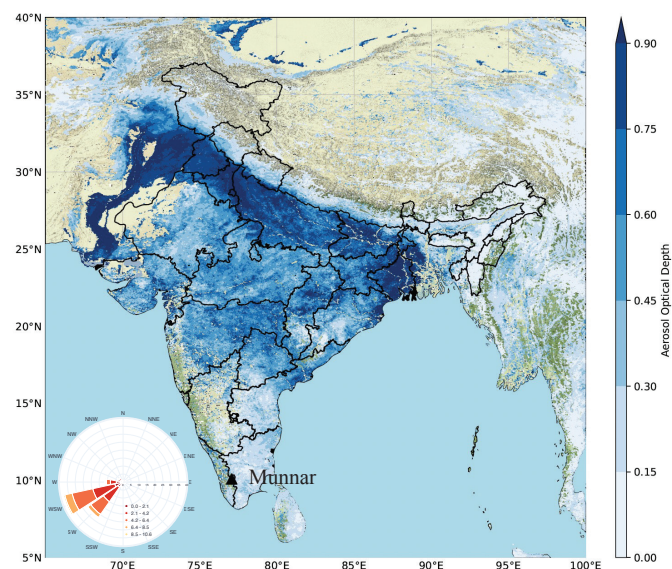
563 Pope, F. D., Dennis-smither, B. J., Griffiths, P. T., Clegg, S. L., & Cox, R. A. (2010). Studies of
564   Single Aerosol Particles Containing Malonic Acid, Glutaric Acid, and Their Mixtures with
565   Sodium Chloride . I . Hygroscopic Growth. *Growth Factors*, 5335–5341.

566 Prenni, A. J., Petters, M. D., Kreidenweis, S. M., DeMott, P. J., & Ziemann, P. J. (2007). Cloud
567   droplet activation of secondary organic aerosol. *Journal of Geophysical Research Atmospheres*,
568   *112*(10). https://doi.org/10.1029/2006JD007963

569 Rastak, N., Pajunoja, A., Acosta Navarro, J. C., Ma, J., Song, M., Partridge, D. G., Kirkevåg, A.,
570   Leong, Y., Hu, W. W., Taylor, N. F., Lambe, A., Cerully, K., Bougiatioti, A., Liu, P., Krejci, R.,
571   Petäjä, T., Percival, C., Davidovits, P., Worsnop, D. R., … Riipinen, I. (2017). Microphysical
572   explanation of the RH-dependent water affinity of biogenic organic aerosol and its importance
573   for climate. *Geophysical Research Letters*, *44*(10), 5167–5177.
574   https://doi.org/10.1002/2017GL073056

575 Reviakine, I., Johannsmann, D., & Richter, R. P. (2011). Hearing what you cannot see and visualizing
576   what you hear: Interpreting quartz crystal microbalance data from solvated interfaces. *Analytical*
577   *Chemistry*, *83*(23), 8838–8848. https://doi.org/10.1021/ac201778h

578 Riipinen, I., Rastak, N., & Pandis, S. N. (2015). Connecting the solubility and CCN activation of
579   complex organic aerosols: A theoretical study using solubility distributions. *Atmospheric*
580   *Chemistry and Physics*, *15*(11), 6305–6322. https://doi.org/10.5194/acp-15-6305-2015

581 Rose, D., Gunthe, S. S., Mikhailov, E., Frank, G. P., Dusek, U., Andreae, M. O., & Pöschl, U. (2008).
582   Calibration and measurement uncertainties of a continuous-flow cloud condensation nuclei
583   counter (DMT-CCNC): CCN activation of ammonium sulfate and sodium chloride aerosol
584   particles in theory and experiment. *Atmospheric Chemistry and Physics*, *8*(5), 1153–1179.
585   https://doi.org/10.5194/acp-8-1153-2008

586 Shi, J., Hong, J., Ma, N., Luo, Q., He, Y., Xu, H., Tan, H., Wang, Q., Tao, J., Zhou, Y., Han, S., Peng,
587   L., Xie, L., Zhou, G., Xu, W., Sun, Y., Cheng, Y., & Su, H. (2022). Measurement report: On the
588   difference in aerosol hygroscopicity between high and low relative humidity conditions in the
589   North China Plain. *Atmospheric Chemistry and Physics*, *22*(7), 4599–4613.
590   https://doi.org/10.5194/acp-22-4599-2022

591 Smith, M. L., Bertram, A. K., & Martin, S. T. (2012). Deliquescence, efflorescence, and phase
592   miscibility of mixed particles of ammonium sulfate and isoprene-derived secondary organic
593   material. *Atmospheric Chemistry and Physics*, *12*(20), 9613–9628. https://doi.org/10.5194/acp-
594   12-9613-2012

595 Smith, M. L., Kuwata, M., & Martin, S. T. (2011). Secondary organic material produced by the dark
596   ozonolysis of-pinene minimally affects the deliquescence and efflorescence of ammonium
597   sulfate. *Aerosol Science and Technology*, *45*(2), 244–261.
598   https://doi.org/10.1080/02786826.2010.532178

599 Smith, M. L., You, Y., Kuwata, M., Bertram, A. K., & Martin, S. T. (2013). Phase transitions and
600   phase miscibility of mixed particles of ammonium sulfate, toluene-derived secondary organic
601   material, and water. *Journal of Physical Chemistry A*, *117*(36), 8895–8906.
602   https://doi.org/10.1021/jp405095e

603 Starzak, M., & Peacock, S. D. (1997). Water activity coefficient in aqueous solutions of sucrose -a
604   comprehensive data analysis. *Zuckerindustrie*, *122*(5), 380–387.

605 Tang, M., Chan, C. K., Li, Y. J., Su, H., Ma, Q., Wu, Z., Zhang, G., Wang, Z., Ge, M., Hu, M., He,
606   H., & Wang, X. (2019). A review of experimental techniques for aerosol hygroscopicity studies.
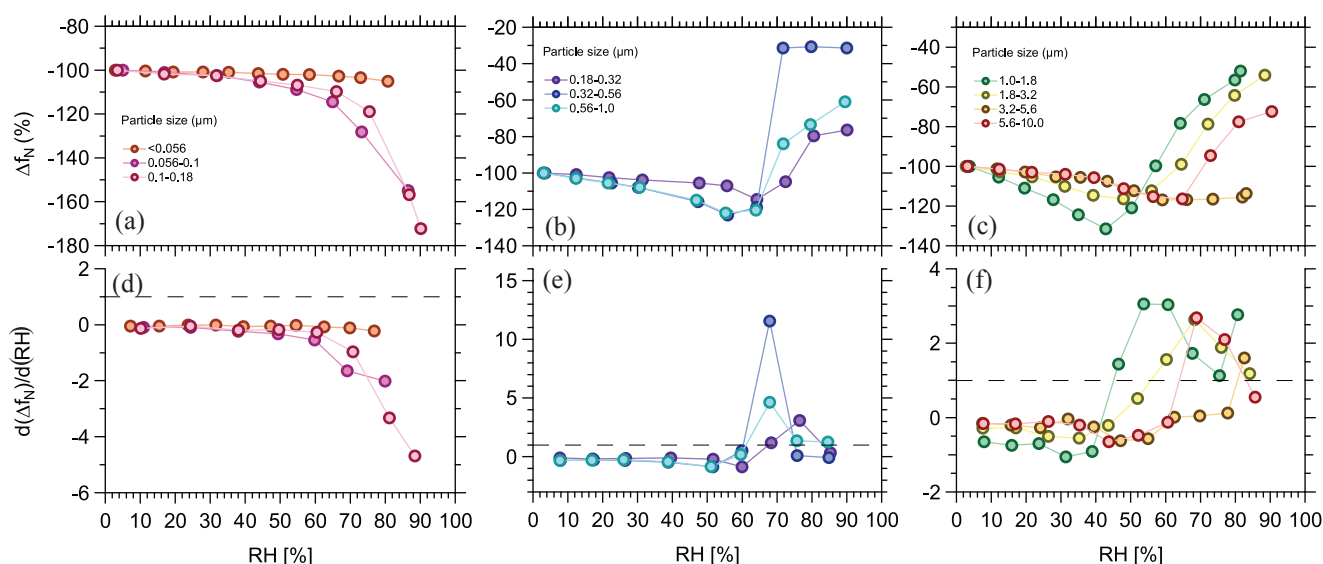
Atmospheric Chemistry and Physics, *19*(19), 12631–12686. https://doi.org/10.5194/acp-19-12631-2019

Valsan, A. E., Ravikrishna, R., Biju, C. V., Pöhlker, C., Després, V. R., Huffman, J. A., Pöschl, U., & Gunthe, S. S. (2016). Fluorescent biological aerosol particle measurements at a tropical high-Altitude site in southern India during the southwest monsoon season. *Atmospheric Chemistry and Physics*, *16*(15), 9805–9830. https://doi.org/10.5194/acp-16-9805-2016

Wang, Y., Li, Z., Zhang, Y., Du, W., Zhang, F., Tan, H., Xu, H., Fan, T., Jin, X., Fan, X., Dong, Z., Wang, Q., & Sun, Y. (2018). Characterization of aerosol hygroscopicity, mixing state, and CCN activity at a suburban site in the central North China Plain. *Atmospheric Chemistry and Physics*, *18*(16), 11739–11752. https://doi.org/10.5194/acp-18-11739-2018

Wang, Z., Cheng, Y., Ma, N., Mikhailov, E., Pöschl, U., & Su, H. (2017). Dependence of the hygroscopicity parameter κ on particle size, humidity and solute concentration: implications for laboratory experiments, field measurements and model studies. *Atmospheric Chemistry and Physics*, *March*, 1–33. https://doi.org/10.5194/acp-2017-253

Wittbom, C., Eriksson, A. C., Rissler, J., Roldin, P., Nordin, E. Z., Sjogren, S., Nilsson, P. T., Swietlicki, E., Pagels, J., & Svenningsson, B. (2018). Effect of solubility limitation on hygroscopic growth and cloud drop activation of SOA particles produced from traffic exhausts. *Journal of Atmospheric Chemistry*, *75*(4), 359–383. https://doi.org/10.1007/s10874-018-9380-5

Wu, Z. J., Poulain, L., Henning, S., Dieckmann, K., Birmili, W., Merkel, M., Van Pinxteren, D., Spindler, G., Müller, K., Stratmann, F., Herrmann, H., & Wiedensohler, A. (2013). Relating particle hygroscopicity and CCN activity to chemical composition during the HCCT-2010 field campaign. *Atmospheric Chemistry and Physics*, *13*(16), 7983–7996. https://doi.org/10.5194/acp-13-7983-2013

Wu, Z. J., Zheng, J., Shang, D. J., Du, Z. F., Wu, Y. S., Zeng, L. M., Wiedensohler, A., & Hu, M. (2016). Particle hygroscopicity and its link to chemical composition in the urban atmosphere of Beijing, China, during summertime. *Atmospheric Chemistry and Physics*, *16*(2), 1123–1138. https://doi.org/10.5194/acp-16-1123-2016

Zhang, S., Shen, X., Sun, J., Zhang, Y., Zhang, X., Xia, C., Hu, X., Zhong, J., Wang, J., & Liu, S. (2023). Atmospheric particle hygroscopicity and the influence by oxidation state of organic aerosols in urban Beijing. *Journal of Environmental Sciences (China)*, *124*, 544–556. https://doi.org/10.1016/j.jes.2021.11.019

Zhao, P., Ge, S., Su, J., Ding, J., & Kuang, Y. (2022). Relative Humidity Dependence of Hygroscopicity Parameter of Ambient Aerosols. *Journal of Geophysical Research: Atmospheres*, *127*(8), 1–10. https://doi.org/10.1029/2021JD035647

Zieger, P., Väisänen, O., Corbin, J. C., Partridge, D. G., Bastelberger, S., Mousavi-Fard, M., Rosati, B., Gysel, M., Krieger, U. K., Leck, C., Nenes, A., Riipinen, I., Virtanen, A., & Salter, M. E. (2017a). Revising the hygroscopicity of inorganic sea salt particles. *Nature Communications*, *8*(July). https://doi.org/10.1038/ncomms15883

Zieger, P., Väisänen, O., Corbin, J. C., Partridge, D. G., Bastelberger, S., Mousavi-Fard, M., Rosati, B., Gysel, M., Krieger, U. K., Leck, C., Nenes, A., Riipinen, I., Virtanen, A., & Salter, M. E. (2017b). Revising the hygroscopicity of inorganic sea salt particles. *Nature Communications*, *8*(May). https://doi.org/10.1038/ncomms15883

649   Zobrist, B., Soonsin, V., Luo, B. P., Krieger, U. K., Marcolli, C., Peter, T., & Koop, T. (2011). Ultra-
650   slow water diffusion in aqueous sucrose glasses. *Physical Chemistry Chemical Physics*, *13*(8),
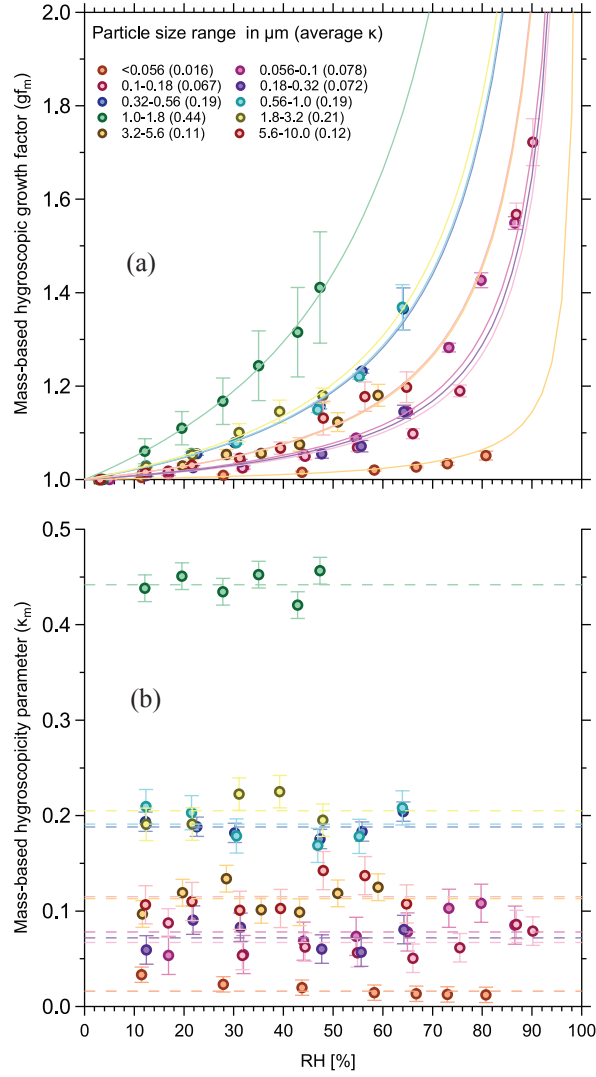651   3514–3526. https://doi.org/10.1039/c0cp01273d

652

Figure.

Figure 1. Spatial distribution of average Aerosol Optical Depth (AOD) derived from MODIS (Moderate Resolution Imaging Spectroradiometer) Level 2 data over the Indian continental region during the monsoon season of 2021 (June - September). The AOD distribution clearly indicates a relatively lower aerosol loading over the observational site of Munnar (marked as a black triangle) compared with the other parts of India. The wind rose diagram shown in the inset is average wind speed and wind direction arriving at the sampling site during the ambient aerosol sampling period (August – September 2021). The prevailing air masses mostly originated over the Indian Ocean and arrived from southwest direction, bringing clean marine influx to the observational site, confirming the relatively low influence of anthropogenic activities.
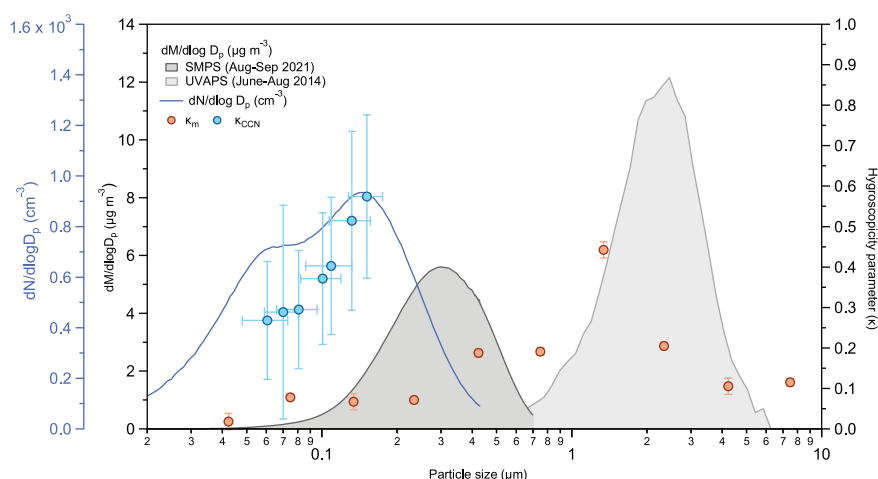
Figure 2. Deliquescence phase transition behaviour of size-resolved ambient aerosol particles from Munnar. For panels a, b, and c, Δf_N represents the change in the oscillation frequency of the quartz crystal microbalance (QCM) sensor resulting due to water uptake by the ambient aerosol particles at different relative humidity (RH) conditions normalised to that of the dry aerosol particles at RH <5%, expressed as percentage. The decrease in the value of Δf_N for each size range for the sampled ambient aerosol particles indicates the water uptake at different RH conditions in the subsaturated regime. The solid markers and lines identify different particle size ranges. In panels d, e, and f the derivative of Δf_N with respect to RH ($d(\Delta f_N)/d(RH)$) is plotted against RH to determine the deliquescence relative humidity (DRH) value corresponding to the respective aerosol size ranges. The RH values at which $d(\Delta f_N)/d(RH)$ becomes ≥ 1 (marked by the dotted line) represent the DRH values for the individual aerosol size ranges.

Figure 3. Size-resolved hygroscopicity measurements of ambient aerosol particles at the high-altitude site, Munnar, during the Monsoon season (August-September 2021). (a) Mass-based hygroscopic growth factor (gf_m) derived using a quartz crystal microbalance (QCM) for ten different size ranges of ambient aerosol particles at different relative humidity (RH) conditions in the subsaturated regime (circles). The solid lines represent the corresponding κ-Köhler growth factor fits obtained using the mean value of mass-based hygroscopicity parameter, $κ_m$. The error bars represent the variations in gf_m averaged over the mass change corresponding to different overtone frequencies of the QCM sensor at respective RH conditions. The values in parentheses are the mean $κ_m$ values corresponding to respective size ranges. (b) The data points are the $κ_m$ values calculated based on the gf_m (as shown in (a)) using the κ-Köhler theory for different RH conditions in the subsaturated regime. The dotted lines represent the mean $κ_m$ value for each size range of ambient aerosol particles and the error bars represent one standard deviation.

Figure 4. Aerosol size distributions, hygroscopicity parameters derived from quartz crystal microbalance (QCM) experiments (κ_m), and from size-resolved cloud condensation nuclei (CCN) measurements (κ_{CCN}). The number size distribution obtained using a Scanning Mobility Particle Sizer (SMPS) over the size range of 10 – 430 nm (blue curve) was measured during the sampling period and exhibited a bimodal distribution. The mass size distributions (dark grey shaded area) were derived based on the aerosol number size distribution by assuming a density of 1.2 g cm^{-3} for the submicron region. The mass size distribution for the supermicron range (light grey shaded area) was obtained using Ultraviolet Aerodynamic Particle Sizer (UV-APS) measurements during the same season (June-August) but for a different year (2014). The hygroscopicity parameters derived from QCM experiments (κ_m; orange points) and size-resolved CCN measurements (κ_{CCN}; blue points) are shown for the comparison. The error bars for κ_m and κ_{CCN} indicate the measurement uncertainty and variability, respectively.